

Electrospray Propulsion Engineering Toolkit (ESPET)

IEPC-2017-206

*Presented at the 35th International Electric Propulsion Conference
Georgia Institute of Technology • Atlanta, Georgia • USA
October 8 – 12, 2017*

Benjamin St. Peter¹ and Rainer A. Dressler²
Spectral Sciences, Inc., Burlington, MA, 02474, USA

Yu-hui Chiu³ and Timothy Fedkiw⁴
Busek Co. Inc., Natick, MA 01760, USA

and

Yi Wang⁵ and Hongjun Song⁶
CFD Research Corporation, Huntsville, AL, 35806, USA

Abstract: We report on the development of a software tool, the Electrospray Propulsion Engineering Toolkit (ESPET), for the design of microfluidic systems of emitter arrays and forecasting their performance. ESPET is a multi-scale model that extends experimental and detailed high-level physics characterization of microfluidic components to full-scale ESP microfluidic network performance. The tool is designed to allow ESP system engineers to efficiently narrow down the system component trade space and thereby substantially reduce the development time of advanced ESP systems of arbitrary design including both dielectric and liquid metal propellants. ESPET takes an engineering model approach that breaks the ESP system down into multiple microfluidic components or domains that can be described by either analytical microfluidic or reduced order numerical solutions. ESPET can be divided into three parts: a central database of critical microfluidic properties, a microfluidic domain modeler, and a microfluidic network solver. The prototype software exploits the Hagen-Poiseuille–Ohm’s Law analogy by using the publicly available SPICE electric circuit simulation software to solve the flow properties of the microfluidic network. The domain modeler produces custom components for SPICE to solve for both microfluidic flow and electrical current of Taylor cones. First tests have been conducted on ionic liquid capillary emitters to demonstrate the ESPET approach.

Nomenclature

A	= field evaporation area
C_R	= dimensionless hydraulic resistance
D	= distance between emitter tip and extractor
D_{eff}	= effective pore size
ΔG	= ion solvation free energy
ΔP	= pressure drop

¹ Research Scientist, bstpeter@spectral.com.

² Chief Scientist, rdressler@spectral.com.

³ Director of Applied Sciences, ychiu@busek.com.

⁴ Research Engineer, tfedkiw@busek.com.

⁵ Director, Biomedical & Energy Technologies, yi.wang@cfdr.com

⁶ Principal Engineer, hongjun.song@cfdr.com

ΔU	= voltage drop
E_{max}	= maximum normal surface field strength on vacuum side of vacuum liquid interface
E_{max}^l	= maximum normal surface field strength on liquid side of vacuum liquid interface
EMI-BF4	= 1- ethyl-3-methylimidazolium tetrafluoroborate
EMI-TFSI	= 1- ethyl-3-methylimidazolium bis(trifluoromethylsulfonyl)imid
EMI-GaCl4	= 1- ethyl-3-methylimidazolium gallium tetrachloride
$G(E)$	= free energy associated with external field, E
γ	= propellant surface tension
ε	= relative permittivity
ε_0	= vacuum permittivity
ϕ	= porosity
h	= Planck constant
I	= electrical current
$I_{droplet}$	= droplet current
I_{ion}	= ion or field evaporation electrical current
I_{min}	= ion evaporation current at onset
I_{sp}	= specific impulse
K	= propellant conductivity
k_B	= Boltzmann constant
κ	= permeability
Q	= volume flow rate
q/m	= charge to mass ratio
R	= electrical resistance
R_{hyd}	= hydraulic resistance
r_{tip}	= tip radius of curvature
r_{base}	= Taylor cone base radius
ρ	= propellant density
σ	= surface charge density
T	= temperature
V	= voltage
V_0	= onset voltage

I. Introduction

ELECTROSPRAY PROPULSION (ESP) has the potential of meeting many miniaturization and specific impulse requirements of propulsion systems for future space missions. Extensive development has been dedicated to scaling up ESP systems to large, high density arrays of electrospray emitters that can match the thrust of other EP systems while offering higher efficiency upon miniaturization¹⁻⁵. Due to the vast trade space in propellants, emitter types, and substrates, finding an optimal design for a specific mission is highly challenging. Substantial research has been invested in understanding the detailed physics associated with specific emitters and the spray properties of Taylor cones in a vacuum⁶⁻¹². It has been demonstrated that the detailed emission physics at the Taylor cone tip can be influenced by the propellant feed system in both liquid metal (field emission electric propulsion, FEEP)¹³⁻¹⁶ and dielectric or colloidal propellant ESP systems¹⁶⁻¹⁸. The successful design of an ESP array, therefore, requires an understanding of the entire microfluidic system from propellant reservoir to the Taylor cone emission site.

To accelerate the development of scaled-up electrospray propulsion emitter array systems with practical thrust levels, we are developing an Electrospray Propulsion Engineering Toolkit (ESPET). ESPET is a multi-scale engineering tool that extends experimental and detailed high-level physics characterization of microfluidic components to full-scale ESP microfluidic network performance. The tool is designed to allow ESP system engineers to efficiently narrow down the system component trade space and thereby substantially reduce the development time of advanced ESP systems. The tool can also be applied to diagnosing prototype systems in a laboratory environment.

ESPET can be divided into three parts: a central database of critical microfluidic properties, a microfluidic domain modeler, and a microfluidic network solver. The physics underlying a microfluidic network of an ESP system covers multiple scale lengths that render the application of high-level computational fluid dynamics (CFD) or atomistic molecular dynamics (MD) simulations over the entire system impractical. ESPET takes an engineering

model approach that breaks the ESP system down into multiple microfluidic components or domains that can be described by analytical microfluidic solutions or reduced order numerical solutions. ESPET will be applicable to dielectric propellant (colloidal systems) and liquid metal (FEED) ESP systems with a variety of emitter type designs, including internally and externally wetted emitters, and porous emitter systems. The goal is to develop a tool that can predict performance estimates for propulsion system designs of arbitrary complexity. Computed performance outputs include thrust, specific impulse (I_{sp}), efficiency, current, mass flow, and array emission uniformity. Uniformity is a critical challenge in current designs, and ESPET predicts uniformity based on the specification of tolerances of various component specifications, such as the pore size distribution of porous emitters, or the distribution of curvatures of externally wetted or porous tips.

In its current form, ESPET is set up as a web application. We envision an interactive development platform where users provide new propellant properties as they become available. It is also possible to set up a proprietary system based on proprietary propellant and substrate data. The most sophisticated domains of the microfluidic network are the emitter components, which incorporate the most recent theory associated with the respective Taylor cone charge emission properties and the respective coupling to the substrate and feed system. The design is modular in order to facilitate upgrades based on the latest research developments. This paper provides an introductory overview of ESPET. In Section 2, we provide a more detailed overview of the ESPET structure. In Section 3, we discuss the three primary ESPET components, the database, the domain modeler, and the network solver. In Section 4 we show how a system can be designed and the performance computed using the freely available SPICE electric circuit solver, where we rely on the Hagen-Poiseuille–Ohm’s Law analogy. We demonstrate this on simple electrospray propulsion systems. In Section 6, we conclude with the status of development and future upgrades.

II. Overview of ESPET

Figure 1 provides an overview of the ESPET structure and functional process flow. An ESPET calculation starts with the division of the envisioned propulsion system into separate domains, and the calculation of domain microfluidic parameters in a domain modeler. The domain modeler relies on a database for propellant, substrate and interfacial properties. For several liquid propellant properties, temperature dependent values are provided in the form of polynomials. The outputs of the domain modeler consist of microfluidic network components that can then be inserted in the network solver. In the current prototype version of ESPET, we use the freely available SPICE electric circuit simulator¹⁹. SPICE has an easy-to-use graphical user interface (GUI) with which electrical circuits can be designed. In ESPET, we apply the Hagen-Poiseuille – Ohm’s Law analogy:

$$\Delta P = R_{hyd} Q \Leftrightarrow \Delta U = RI . \quad (1)$$

Thus, ESPET sets up SPICE to solve for the volume flow rate, Q , or the mass flow rate, $\dot{m} = Q\rho$, where domains consisting of fluidic conduits are characterized by their hydraulic resistance, and domains such as a propellant reservoir may be characterized by a pressure. A critical difference with respect to electrical circuits is that output flow rate can only have a single, positive polarity. As discussed further below, a primary challenge in applying SPICE to the electrospray problem is the necessity to determine both microfluidic output flow and electrical output current. We accomplish this by designing, through our domain modeler, smart components with multiple outputs (both microfluidic and electrohydrodynamic). The components incorporate the physics of specific emitter designs.

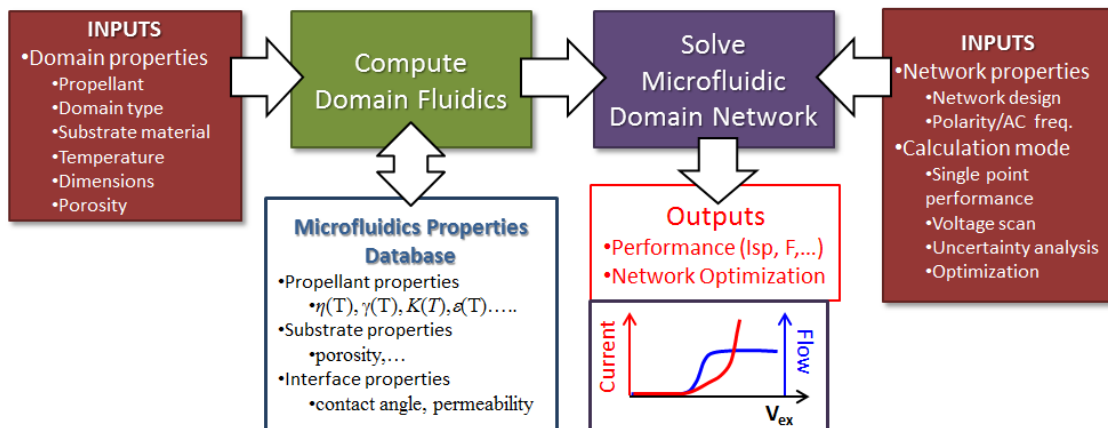


Figure 1. Overview of ESPET structure and process flow.

Using the SPICE GUI, the user can then control the outputs of ESPET. This is further discussed below. The smart components, in addition to providing output flow and current, also provide outputs such as emitter thrust, specific impulse and polydispersive efficiency. These outputs can be produced as a single extraction voltage output, or an extraction voltage scan, such as the production of a voltage-current (VI) curve, which is graphically displayed. The user can also exploit special features of the SPICE simulator such as circuit optimization and the calculation of uncertainty bounds based on tolerances of properties provided by the user. The ESPET domain modeler and database are accessed through a web interface. The user has to separately download SPICE, for example the LTspice version from Linear Technologies²⁰. In the subsequent sections, we discuss each ESPET component in greater detail.

III. ESPET Components

A. Microfluidics Properties Database

At the core of ESPET is a database of microfluidic properties. A schematic of the database structure and how entries are managed is shown in Figure 2. The database has three tables for propellant, substrate and interfacial properties. Most of the properties are accompanied by metadata which include temperature validity ranges and references to the data sources. The database is run by the frequently used SQLite database engine. For users not familiar with SQLite²¹, new entries can be entered in an Excel database entry template, which is then converted to SQLite with a utility.

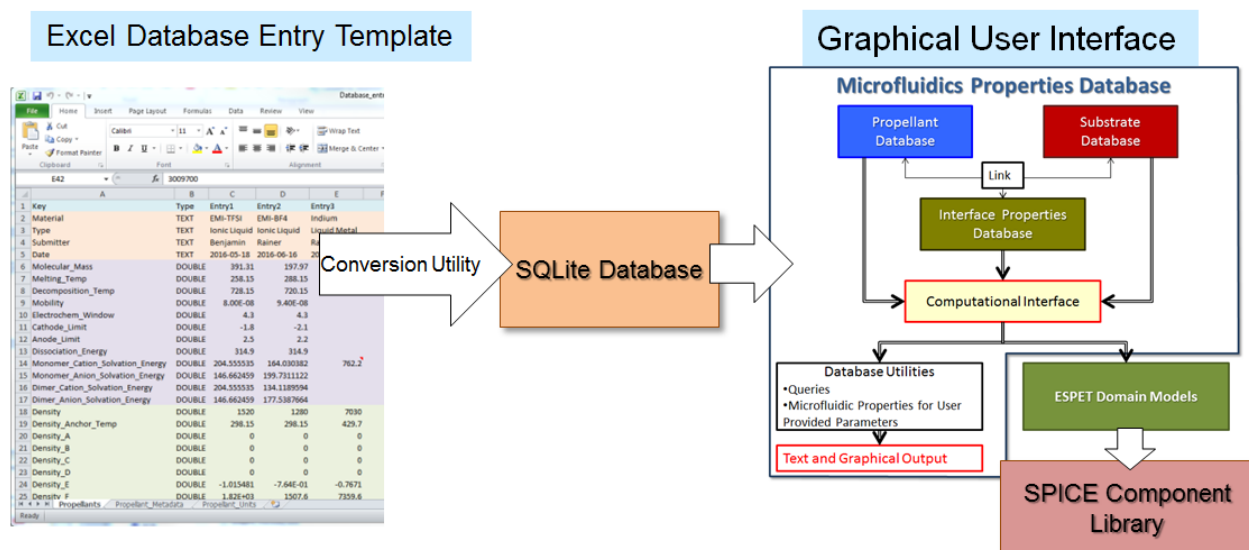


Figure 2. ESPET microfluidic properties database structure.

The database is integrated in a web interface including a propellant property visualization utility and the domain modeling utility for the development of microfluidic components for eventual placement in an electrospray system microfluidic network. The propellant visualization utility allows the user to cross-compare properties of propellants. Figure 3 shows a screenshot of the database utility where the temperature dependence of the dynamic viscosity is plotted for the four propellants currently in the database, the ionic liquids EMI-TFSI, EMI-BF4, EMI-GaCl4, and the liquid metal, indium. The visualization can be filtered using the SQLite search engine. In the example of Fig. 3, an open search not specifying the type (ionic liquid or liquid metal) and entry date, and looking for all propellants with melting temperature greater than or equal to 250 K is shown. The text box below the filter includes the metadata for the displayed data. Other properties with temperature dependencies that can be visualized are relative permittivity, density, and conductivity. The user can export the chart data to a csv file.

Following substrates are currently included in the substrate database: borosilicate glass (non-porous), borosilicate glass fibermat, six grades of porous borosilicate, rhenium, silicon, stainless steel, xerogel, and two grades of porous tungsten. Data including interfacial data are obtained either from the literature, or from measurements at Busek Company. Data entries include density, conductivity, porosity, roughness and relative permittivity. Interfacial properties are listed for substrate-propellant pairs, where available, and include contact angle and effective pore size for porous substrates. The effective pore size is related to the substrate permeability through^{22,23}:

$$\kappa \approx D_{eff}^2 \{240(1 - \phi)^2\}^{-1}. \quad (2)$$

Domain Modeler

The domain modeler is a web-based modeling utility for the design of microfluidic components for eventual placement in an electrospray system network. The user designs a specific domain and then microfluidic properties of the domain are computed and displayed. The properties are computed with direct access to the properties database. There are two types of domains, feed system domains and emitter domains. Feed system domains include various flow media including cylindrical (capillary) or rectangular open channels, or porous media of similar shapes. Emitter domains incorporate the liquid Taylor cone charge emission physics, and the effects of the substrate on the Taylor cone base.

1. Feed System Domain Models

The flow properties in feed system domains are computed with analytical viscous flow models or reduced order numerical solutions assuming laminar flow and channel dimensions below the capillary limit for which gravity can be neglected. Figure 4 shows a screenshot of the setup of a viscous flow feed domain consisting of a tapered porous conduit. On the left, the user selects options for the domain type, substrate, propellant and temperature range. The entries for the domain shape and porosity properties are entered to the right of the domain shape design that defines the input variables. Once a property (Field) is selected, a plot of the temperature dependence of this property is obtained by clicking “Run”. The chart shows the temperature dependence of the hydraulic resistance (in units of Pa s/ μ L) of the porous medium in the defined flow direction. In order to export the component to a SPICE component library, the user clicks “Save”, and the component is saved with microfluidic properties at the temperature Tmin. Not shown in Fig. 4 is the metadata text box providing information on how the various properties are computed. For viscous flow domains, the user can select in the “Field” box additional properties, including Laplace pressure, wicking time, flow rate and mass flow induced by the Laplace pressure as the conduit becomes fully wicked, and the Reynolds number.

2. Emitter Domains

In order to set up an emitter component, the user selects an emitter type consisting of a Taylor cone substrate base design. The emitter domains are the most challenging problem of ESPET and are still under development. Table 1 lists the current emitter types, the status of development, and references used to develop the utility and component models. To date, we have only developed the models for ionic liquid emitters. Models for liquid metal emitters will be included in the future. We differentiate between emitter utilities and component models which are integrated in an exportable SPICE component. ESPET utilities compute emitter properties for a specified volume

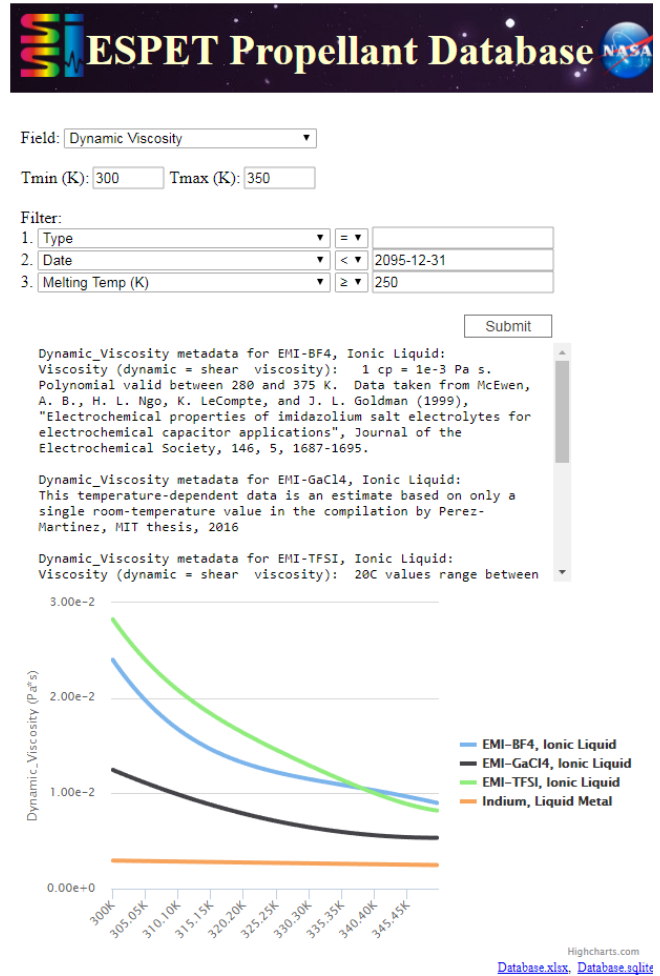


Figure 3. Screenshot of ESPET database web utility.

flow rate at the onset voltage assuming a cone-jet mode of operation. The default flow rate is given by the minimum flow rate at which a Taylor cone-jet can be sustained¹²:

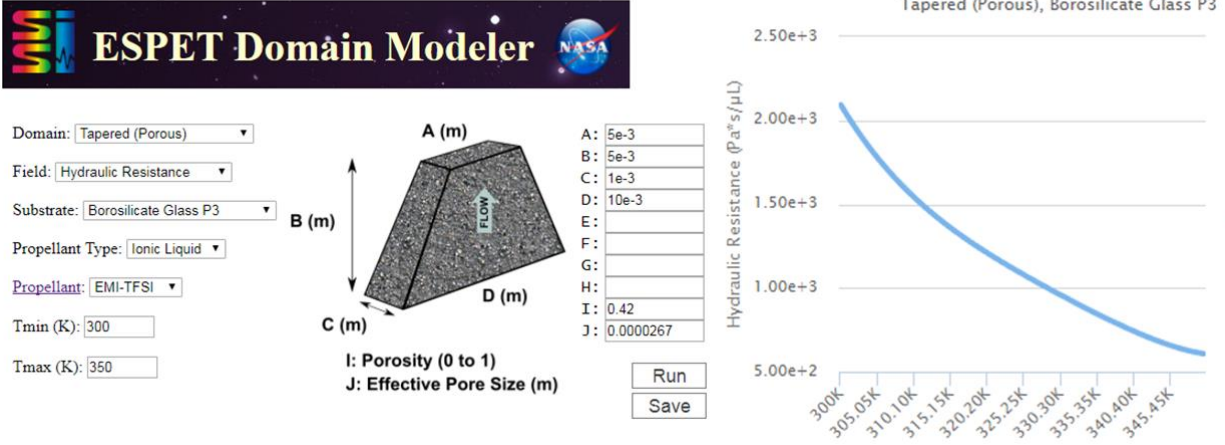


Figure 4. Screenshot of domain modeler with setup for the design of a porous feed component.

Table 1. Development status of emitter types currently available in ESPET.

Emitter Type	ESPET Domain Name	Status	References
Capillary (internally wetted)	Taylor Cone (Capillary)	Ionic liquid Utility and component	12, 13, 17, 18, 24-27
Conical porous tip	Taylor Cone (Porous)	Ionic liquid Utility and component	2, 3, 28
Porous edge	Taylor Edge (Porous)	Ionic liquid Utility and component	16
Conical externally wetted	Taylor Cone (Ext Wetted)	Ionic liquid Utility	12, 13, 17, 18, 24-27
Edge externally wetted	Taylor Edge (Ext Wetted)	Ionic liquid Utility	12, 13, 17, 18, 24-27

$$Q_{\min} = \frac{1}{4} \frac{\gamma \varepsilon \varepsilon_0}{\rho K} . \quad (3)$$

Utility outputs include the onset voltage (computed from expressions reported in the literature), hydraulic resistance of the emitter, the minimum flow rate, the droplet and ion currents, the spray charge to mass ratio, thrust, I_{sp} , the maximum surface electric field, the mass flow, and the polydispersive efficiency. A screenshot of the capillary Taylor cone emitter domain modeler is shown in Fig. 5. It illustrates the required user inputs for estimating individual emitter performance and for developing a SPICE component. Note that for this model the user needs to define the polarity of the emitter (Parameter F in Fig. 5). Future models may include emitters with alternating polarity for time-dependent network modeling.

The droplet current, $I_{droplets}$, is computed from the empirical expression derived by Gañán-Calvo *et al.*²⁹:

$$I_{droplet} = \sqrt{\frac{\varepsilon_0 \gamma^2}{\rho}} \left[6.2 \sqrt{\frac{Q \rho K}{\gamma \varepsilon_0 \sqrt{\varepsilon - 1}}} - 2 \right] = I_0 \left[6.2 \sqrt{\frac{Q}{Q_0 \sqrt{\varepsilon - 1}}} - 2 \right] \quad (4)$$

$$Q_0 = \frac{\gamma \varepsilon_0}{\rho K}, I_0 = \sqrt{\frac{\varepsilon_0 \gamma^2}{\rho}}$$

The maximum cone-jet surface field is obtained from¹¹:

$$E_{\max} = \frac{\gamma^{1/2} K^{1/6}}{\varepsilon_0^{2/3} Q^{1/6}} . \quad (5)$$

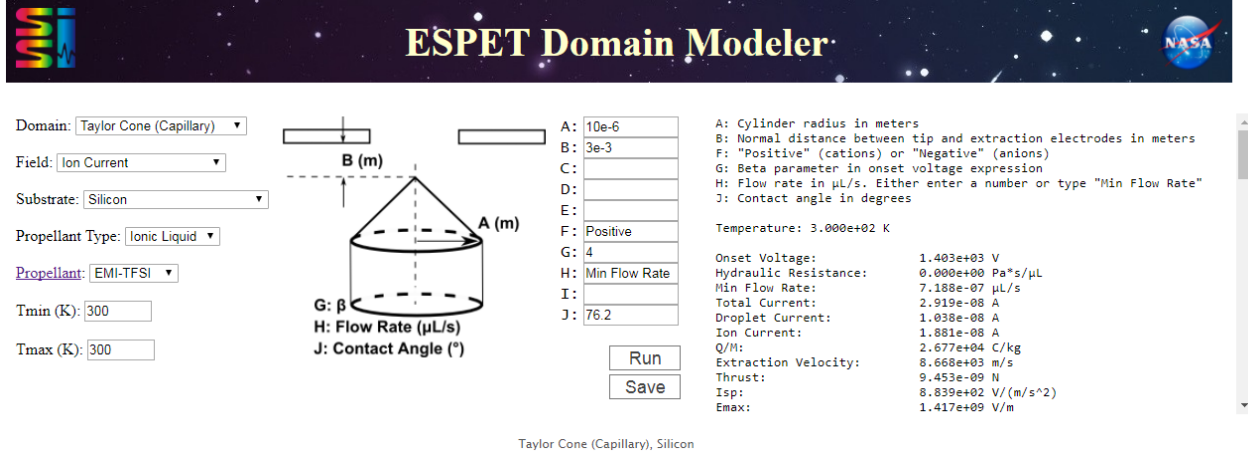


Figure 5. Screenshot of domain modeler with setup for the design of a capillary emitter.

We then follow the ion field evaporation theory of Higuera²⁴ and Coffman¹⁷ to compute the ion field evaporation current assuming field evaporation occurs at the neck of the cone-jet from:

$$I_{ion}(E_{max}) = A(E_{max})\sigma(E_{max})\frac{k_B T}{h} \exp\left[-\frac{\Delta G - G(E_{max})}{k_B T}\right], \quad (6)$$

where the effective field evaporation area, $A(E_{max})$, is estimated from:

$$A(E_{max}) = \pi r_e^2, \quad r_e = \frac{4\gamma}{\epsilon_0 E_{max}^2}. \quad (7)$$

Coffman justifies that the convection current can be neglected in the field evaporation region near the Taylor cone tip. In this case the field evaporation current is equal to the conduction current given by:

$$I_{ion}(E_{max}) = A(E_{max})KE_{max}^l \quad (8)$$

and the internal electric field, E_{max}^l , can be computed assuming a steady-state surface charge density from:

$$E_{max}^l = \frac{E_{max}}{\epsilon \left(1 + \frac{hK}{\epsilon_0 \epsilon k_B T} \exp\left[-\frac{1}{k_B T} \{\Delta G - G(E_{max})\}\right] \right)}. \quad (9)$$

This approach neglects ion emission at the jet tip. Measurements by Gamero-Castaño³⁰ have observed a substantial ion current fraction at high flow rates of a EMI-TFSI system, and concluded that ion emission occurs primarily at the jet tip. At high flow rates, E_{max} is too low for measurable field evaporation. Inclusion of jet tip ion emission will be incorporate in a future ESPET upgrade.

For component models, we exploit an arbitrary function generator feature in SPICE that allows the user to develop custom components. This enables the development of Taylor cone components that produce both flow as well as electric current output, while the network is operated in a Hagen-Poiseuille mode.

Component models for the SPICE network solver follow similar physics as the domain modeler utility. However, they require that the microfluidic network provide input flow and pressure as a function of extraction field strength. This is straightforward for actively pressurized systems where the flow rate is given by the ratio between the pressure drop across the feed system and the feed system hydraulic resistance. The first emitter component that we developed was for an actively pressurized capillary emitter. Figure 6 shows the component, identified as TC, as it appears after insertion in a schematic in the LTspice GUI. The extraction voltage and the boost or acceleration voltage are set by connecting the input tabs to voltage sources. If the extraction voltage exceeds the onset voltage, the emitter emits current based on equations (4-9). The component computes the I_{sp} , thrust, mass flow, q/m , the total current, and ion and droplet currents, and the polydisperse efficiency. All of these outputs are available to the graphics and plot functions of SPICE.

For passively pressurized emitters, the electric field drives the flow. In a cone-jet mode, we compute the field-induced pressure to produce flow as an excess pressure beyond the onset voltage, as proposed by Perez-Martinez³¹:

$$\Delta P \approx \frac{2\varepsilon_0(V^2 - V_0^2)}{a^2 \operatorname{atanh}^2(\eta)(1 - \eta^2)^2}, \quad (10)$$

$$a = 2D/\eta, \quad \eta = (1 + r_{ip}/D)^{-1/2}.$$

For emitters in a pure ionic regime, we follow the work by Coffman *et al.*¹⁸. This is still an area of active research and there are no simple analytical formulae that predict that a Taylor cone operates in a pure ionic regime. Both for dielectric as well liquid metal propellants, it is known that pure ion emission is more probable for feed systems with high hydraulic resistance^{13,16,18}. Coffman and coworkers¹⁸ determined that the ion evaporation current for dielectric propellants with significant conductivities is inversely proportional to a dimensionless feed system hydraulic resistance parameter, C_R :

$$I_{ion} = I_{min} + \frac{B}{C_R}(V - V_0), \quad (11)$$

$$C_R = \frac{KE_c r_{base}^2}{p_c \rho(q/m)} R_{hyd}, \quad E_c = \sqrt{2p_c / \varepsilon_0}, \quad p_c = 2\gamma / r_{base},$$

where B is a slope parameter that Coffman *et al.* suggest is universal, i.e., applies to all dielectric propellants that operate in a conduction limited regime. (Liquid metals are known to operate in a space charge limited regime¹⁰). We have collected data from recent single emitter measurements in the pure ionic regime conducted in the group of Lozano at MIT. The measurements include a newly identified substrate consisting of a xerogel with very narrow pore-size distribution^{28,31}. We also include measurements by Guerra-Garcia *et al.*³² using borosilicate tips. Figure 7 plots the experimental I-V slopes against $1/C_R$ in order to determine the universal value of B . The data are in polarity pairs and show that only the EMI-BF4 results can be reasonably subjected to a linear regression. The derived slope for EMI-BF4 measurements corresponds to a value of $B = 6.06 \times 10^{-9} \Omega^{-1}$. The time-of-flight measurements conducted by Perez-Martinez³¹ demonstrate that the EMI-TFSI systems operate in a cone-jet mixed ion-droplet regime and the relations in Eq. (11) for pure-ionic regime are thus not applicable.

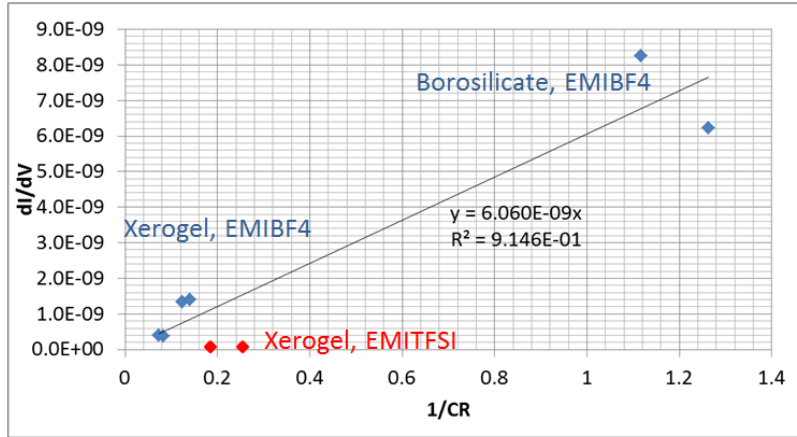


Figure 7. I-V slopes versus $1/C_R$ plotted for recent experimental results from the group of Lozano^{28,31,32}. Slope is taken for EMI-BF4 results only.

The results in Fig. 7 raise the question whether the B slope value is indeed universal, and whether C_R can be used to identify a transition value from mixed to pure-ionic emission. The data in Fig. 7 suggests that EMI-BF4 can operate in pure ionic regime at lower values of C_R than EMI-TFSI. Additional single emitter measurements are planned at Busek to further investigate the utility of Eq. (11) for the pure ionic regime. Currently we propose a threshold value of $C_R \approx 1$ for EMI-BF4, and of at least 10 for EMI-TFSI. We also note that the numerical calculations by Coffman *et al.*¹⁸ focused on systems with $C_R \geq 1,000$, which is a regime normally applicable to externally wetted systems.

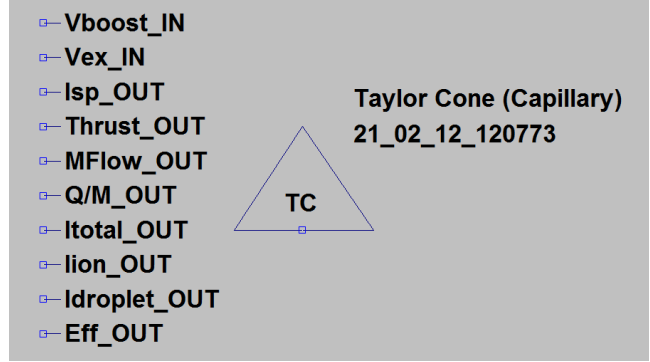


Figure 6. Actively pressurized capillary emitter component as it appears in a network solver (LTspice) schematic.

Porous emitters have the additional complication of multiple emission sites per emitter. Edge emitters can have hundreds of emission sites per centimeter. For typical ionic-liquid contact angles, emission sites are located at specific pores in areas of high surface curvature. Because both the pore size and curvature are subject to distributions, each emission site has a different onset voltage. As the voltage is raised, the number of emission sites increases. Unlike the single emitter IV curves, which are close to linear, those of porous edge emitters or porous tip arrays have a quadratic appearance^{2,16}. We are currently testing an ESPET model for porous emitters where the user specifies the number of emission sites and the standard deviation of Taylor cone base radii about an average value. Note that the Taylor cone base radii can be greater than the pore size for highly wetting propellant/substrate combinations (small contact angles). ESPET determines the actual radii for each emission site from normally distributed random numbers. As the extraction voltage is raised, only those emission sites are active where the voltage exceeds the onset voltage determined from the Taylor cone base radius. The emitter model also takes into account the effect of internal pressure at the emission site, which, in the case of negative pressures, can increase the q/m value of the spray¹⁶. The model will be benchmarked with laboratory measurements of single porous emitters at Busek.

Network Solver

As mentioned earlier, the network solver uses the freely available SPICE electric circuit solver software. SPICE has the advantage of using a mature user interface with a range of simulation and output options. The GUI facilitates setting up a microfluidic network consisting of components such as microfluidic transport channels, pressurized reservoirs, and Taylor cone emitters. Using the Hagen-Poiseuille–Ohm’s Law analogy, the liquid conduits are representative of resistors and pressurized reservoirs are the equivalent of a voltage source. The user can also add a hydraulic capacitance or compliance through the use of a capacitor, which is useful for simulating time-dependent behavior. Currently, we do not have a domain model for producing a compliance component. The user must compute its value and enter the value in the SPICE circuit. As mentioned in the previous section, Taylor cone emitters require specialized components since they operate both in an electrical and a microfluidic domain. For both hydraulic resistances and Taylor cones, the domain modeler computes its properties associated with a chosen propellant, substrate, and temperature. These properties are then saved into a SPICE component file that is transferred to a library of components that SPICE identifies when the user enters a new component to the system schematic.

IV. ESPET Demonstration

In this section we demonstrate the functionality of ESPET by making performance predictions for a simple single-emitter system and a small array. We start with the simplest electro spray thruster design, an actively pressurized capillary emitter. We compare to the data published by Gamero-Castaño and Hruby³³ for a thruster very comparable to the colloid thruster used on the ST-7 Lisa Pathfinder mission³⁴. The LTspice schematic of a single emitter system is shown in Fig. 8. It consists of a pressurized reservoir, a capillary feed system, and a Taylor cone emission site at the end of the capillary emitter. The actively pressurized thruster operates at a single extraction voltage at which Taylor cone stability and emission is optimized. Thrust is adjusted with the acceleration or boost voltage and the mass flow is controlled by the pressure applied to the propellant reservoir. The Taylor cone is modeled in an on-off mode, where the spray properties are constant with extraction voltage above the onset voltage computed for the capillary/extractor geometry defined in the domain modeler (right side of figure). The voltages are applied to the inputs using LTspice voltage source components. We apply a negative 200 V boost voltage which represents the estimated energy lost by droplets in the jet. The total acceleration is given by $V_{ex} + V_{boost}$. The thruster is only operated in a positive current mode.

The feed system consists of custom components for a reservoir and a capillary. These components are generated by the domain modeler that is linked to the microfluidics database. Alternatively, the reservoir can be replaced by a voltage source, which is the equivalent of a pressure source in the microfluidic

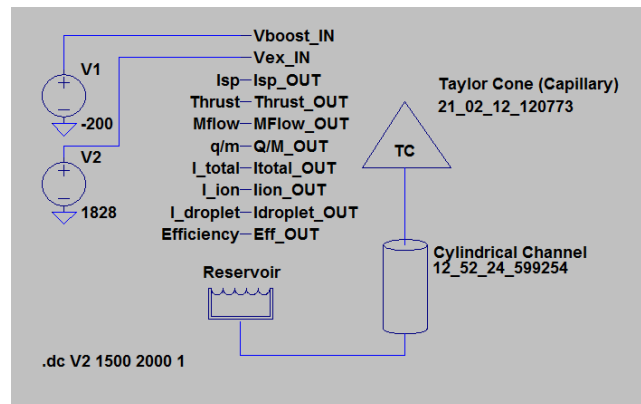


Figure 8. Single capillary emitter thruster schematic in LTspice.

realm. For both options, the user enters pressure in units of Pascal. Flow and hydraulic resistance units are $\mu\text{L/s}$ and $\text{Pa}\cdot\text{s}/\mu\text{L}$, respectively.

Table 2 shows the output results for two input pressures that produced mass flows equivalent to those used when testing the Busek capillary colloid thruster with a EMI-TFSI propellant³³. The pressure was adjusted to match the quoted mass flow. The authors did not accurately specify the length of their capillary feed system. The only substantial discrepancy is observed in the predicted versus experimentally derived thruster efficiency, where the ESPET inefficiency is only based on the assumed 200 V loss of extraction voltage due to Ohmic losses in the jet. The polydisperse efficiency, attributable to the distribution of q/m values in the accelerated spray, is close to 1 since at the respective high flow rates, ion evaporation is predicted to be very low. Additional inefficiency is introduced through beam divergence. The higher experimental inefficiency is consistent with the lower thrust and I_{sp} observed in the experiments. Overall, however, the agreement is very satisfactory.

Table 2. Comparison between ESPET predictions and Busek measurements for an EMI-TFSI propelled single capillary thruster.

Property	ESPET	Busek	ESPET	Busek
Pressure (Pa)	4,100		1,600	
Thrust (μN)	0.78	0.63	0.38	0.35
I_{sp} (s)	147	126	185	171
q/m (C/kg)	636	625	1008	820
Mass flow (mg/s)	0.54	0.54	0.21	0.21
I (mA)	0.34	0.31	0.21	0.22
Extraction Voltage (V)	1,828	1,828	1,828	1,828
Efficiency (%)	89	68	89	68

In order to test the model in a low flow rate regime that approaches the minimum flow rate, we instructed SPICE to scan a range of low reservoir pressures corresponding to a volume flow rate scan near the minimum flow rate. Figure 9 plots the total, ion, and droplet currents versus the volume flow rate as produced by the Taylor cone SPICE component. The vertical dashed line identifies the minimum flow rate (Eq. 3). The ion field evaporation current is observed to increase below flow rates of $6 \times 10^{-6} \mu\text{L/s}$. Slightly above the minimum flow rate, the ion and total currents reach a maximum. This contradicts what is found experimentally^{11,33}, where the ion field evaporation current continues to increase with decreasing flow rate. We believe that in this regime of high surface electric fields, the applicability of the assumptions underlying Eqs. (5-9) is no longer guaranteed. The theory for this transition region will be upgraded as new models become available. Nevertheless, the current model identifies the transition region from nearly pure droplet regime to an increasing ion evaporation fraction of the total output current.

Figure 10 shows similar plots from the same scan for thrust, I_{sp} , q/m , and polydisperse efficiency. For the latter, we assume that the ion current is composed of equal fractions of monomer (single ion) and dimer (ion complexed with an ion pair) ions. As expected, the thrust increases with flow rate, while the I_{sp} decreases. Thrust and I_{sp} are related to the average q/m of the spray, which declines with flow rate. At the highest flow rate of the chart, the polydisperse efficiency is close to 1 because ESPET predicts that the spray is almost entirely due to droplets. The efficiency decreases as the spray becomes increasingly a mixture between droplets and ions with decreasing flow rate. At the lowest

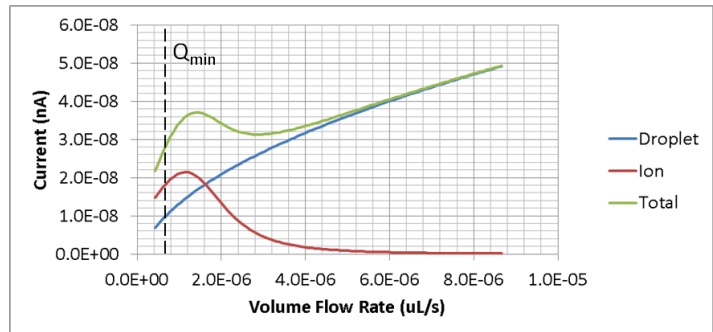


Figure 9. Droplet, ion, and total current versus volume flow rate for a single capillary system using an EMI-TFSI propellant.

flow rate, the efficiency is about 50% due to still significant presence of charged droplets in the spray (see Fig. 9).

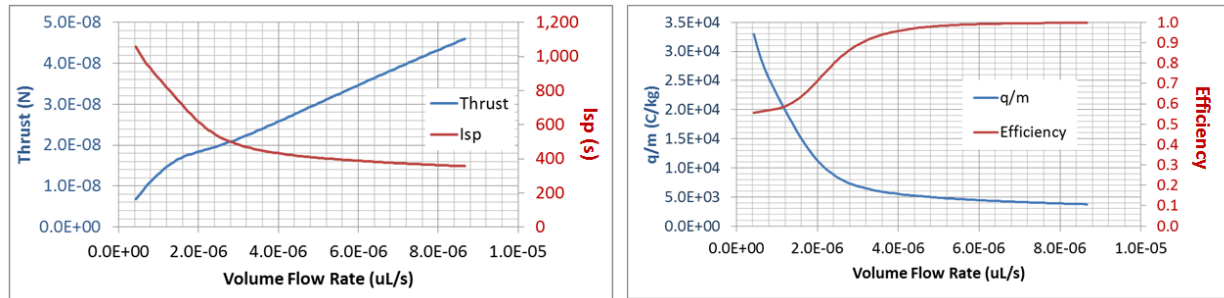


Figure 10. ESPET outputs for thrust and I_{sp} (left frame) and q/m and efficiency (right frame) outputs for system shown in Fig. 8.

In order to demonstrate the ease with which an array can be set up and tested, we show in Figure 11 the schematic of an array of three emitters which is rapidly generated from the schematic of a single thruster in Fig. 8. It would have been trivial to add any number of additional emitters, however, the chart would have been less legible. In Fig. 12 we show the total thrust and I_{sp} of the system as a function of the acceleration voltage. The latter is scanned from 0 to 500 V, while keeping the extraction voltage constant at 1,828 V. The system is operated at a 4,100 Pa reservoir pressure (see Table 2). We still assume a -200 V potential drop in the jet.

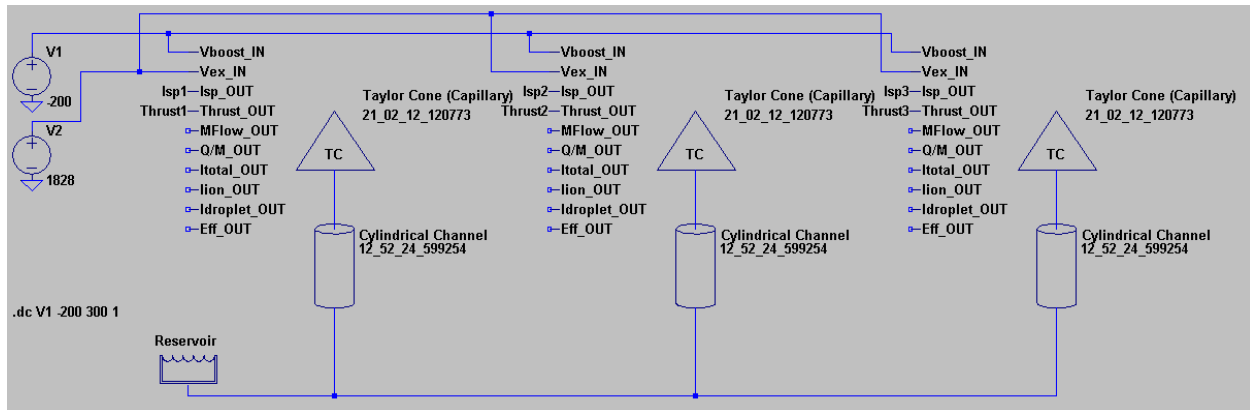


Figure 11. Schematic of three emitter array microfluidic network.

We conclude by applying a powerful feature of LTspice, the built-in Monte Carlo analysis feature. ESPET is designed so component parameters can be associated with tolerances, and the actual parameter value is then set through a random number generator reflecting the 1σ tolerance. To demonstrate this, we associate the hydraulic resistances of the feed capillaries in the network of Fig. 11 with a 10% tolerance. The user can then choose a number of Monte Carlo “trajectories” to compute the distribution of possible performance outcomes. In Figure 13, we show the thrust versus acceleration voltage curves of the three individual emitters in Fig. 11 for a single trajectory where the hydraulic resistance of each capillary was randomly selected once. The figure shows that the thrust of individual emitters vary by approximately 10%. This example illustrates the high precision required for a uniformly emitting array consisting of capillary emitters if the emitters determine the feed system overall hydraulic resistance. The hydraulic resistance is proportional to r^{-4} , where r is the capillary inner radius. Thus, in order to attain a 1σ accuracy of 10% in hydraulic resistance, the inner radius tolerance needs to be 2.5%. This is comparable to the tolerances quoted for microfabricated capillary arrays by Dandavino³⁵. For porous

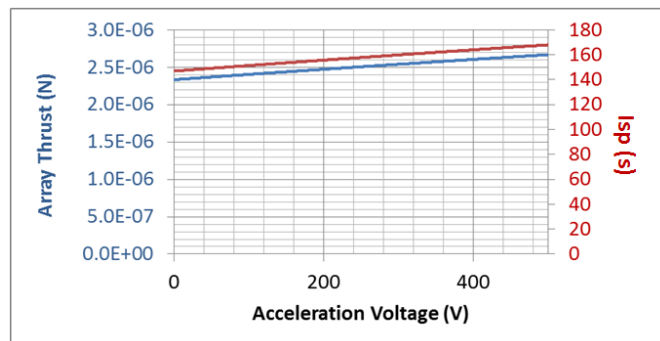


Figure 12. Total thrust and I_{sp} versus acceleration (boost) voltage for 3 emitter array shown in Fig. 11.

emitter domain models, additional non-uniformity can come from the distribution of tip/edge curvatures and pore sizes, which affect the onset voltage. Thus, ESPET in conjunction with the LTspice Monte Carlo feature is well suited for predictions of the emission uniformity of new electro spray array designs.

In addition to a Monte Carlo analysis, LTspice also offers “worst-case” analysis, where the network performance is computed at the extremes of component values specified with a tolerance. This provides for a more direct way of extracting quantitative information on the range of outputs of emitter components.

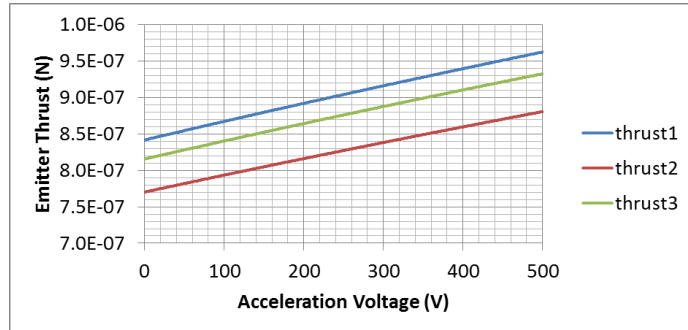


Figure 13. Results from an LTspice Monte Carlo run of the microfluidic network in Fig. 11.

V. Summary and Future Directions

We have developed a framework for multi-scale modeling of electro spray systems that includes both the entire microfluidic feed system and the emitter and associated Taylor cone physics. ESPET applies to the efficient Taylor cone emission mode and will incorporate both dielectric (e.g., ionic liquid) and liquid metal (FEEP) propellant systems. ESPET is designed to allow electro spray system developers to rapidly compute estimates of performance based on a microfluidic network and an electro spray emitter design, and to efficiently explore the large trade space between choice of propellant, substrates, and optimal operational temperature. The latter is particularly important for ionic liquid systems, where conductivity and dynamic viscosity are highly dependent on temperature. ESPET is based on a database of microfluidic properties associated with propellants, substrates, and their interfacial properties, and is set up with an easy-to-use interface to the SPICE electric circuit solver software for microfluidic network design, solution, analysis and outputs.

We report first successful tests on simple ionic liquid electro spray systems involving capillary emitters. Future development includes implementation and testing of porous emitters which are becoming a preferred substrate for both dielectric² and liquid metal emitters³⁶⁻³⁸. These emitters have the added complication of being passively driven with multiple emission sites per emitter that have variances in emitter performance based on pore size distributions. The models for the ionic liquid porous system relies on extensive research from the group of Lozano^{2,3} and more recently in the group of Shea^{16,39}, as well as measurements conducted as part of this project at Busek. Of particular interest is control of the Taylor cone emission properties through the Taylor cone internal pressure and feed system hydraulic resistance^{16,18}. A robust model to identify conditions leading to pure-ionic emission for arbitrary propellants is still necessary. Until such a model is available, empirical approaches will be necessary. Additional features to be developed for dielectric systems include an alternating, time-dependent polarity mode, which will require the addition of new components such as hydraulic capacitances, and predictions of electrochemical decay times. We will also explore the possibility of estimating additional sources of inefficiency to the polydisperse efficiency, such as energy inefficiency due to ohmic losses in the cone-jet transition region, divergence losses, ionization efficiency affected by decay of complex ions in the acceleration region (e.g., dimer, trimer ions), and extraction efficiency (losses on extractor electrode).

The current database already includes properties for a preferred liquid metal propellant, indium. Unlike dielectric systems, which are conductance limited, liquid metal sprays are space-charge limited, and thus follow different physics. Emitter components for capillary (internally wetted), externally wetted, and porous emitters will be developed based on the theoretical and experimental work by Mair, Forbes and Tajmar^{13,14,25-27}.

Acknowledgments

This work has been supported by a NASA Small Business Innovative Research (SBIR) grant under contract No. NNX16CC23C, technical monitor: Dr. John T. Yim. We are grateful to Prof. Paulo Lozano of the Massachusetts Institute of Technology for many helpful discussions and for sharing his research results.

References

- ¹ Dandavino, S., Ataman, C., Ryan, C.N., Chakraborty, S., Courtney, D., Stark, J.P.W., and Shea, H., "Microfabricated electrospray emitter arrays with integrated extractor and accelerator electrodes for the propulsion of small spacecraft," *J. of Micromechanics and Microengineering*, Vol. 24, No. 7, 2014, pp. 075011.
- ² Courtney, D.G., Li, H.Q., and Lozano, P., "Emission measurements from planar arrays of porous ionic liquid ion sources," *J. of Phys. D: Appl. Phys.*, Vol. 45, No. 48, 2012, pp. 485203.
- ³ Legge, R.S., and Lozano, P.C., "Electrospray propulsion based on emitters microfabricated in porous metals," *J. of Propulsion and Power*, Vol. 27, No. 2, 2011, pp. 485-495.
- ⁴ Gassend, B., Velasquez-Garcia, L.F., Akinwande, A.I., and Martinez-Sanchez, M., "A Microfabricated Planar Electrospray Array Ionic Liquid Ion Source With Integrated Extractor," *Microelectromechanical Systems, Journal of*, Vol. 18, No. 3, 2009, pp. 679-694.
- ⁵ Velasquez-Garcia, L.F., Akinwande, A.I., and Martinez-Sanchez, M., "A Planar Array of Micro-Fabricated Electrospray Emitters for Thruster Applications," *J. of Microelectromechanical Systems*, Vol. 15, No. 5, 2006, pp. 1272-1280.
- ⁶ Taylor, G.I., "Disintegration of water drops in an electric field," *Proc. Royal Soc. A*, Vol. 280, No., 1964, pp. 383-397.
- ⁷ Fernández de la Mora, J., "The effect of charge emission from electrified liquid cones," *J. of Fluid Mechanics*, Vol. 243, No., 1992, pp. 561-574.
- ⁸ Fernández de la Mora, J., "The fluid dynamics of Taylor cones," *Annual Review of Fluid Mechanics*, Vol. 39, No., 2007, pp. 217-243.
- ⁹ Fernández de la Mora, J., and Loscertales, I.G., "The current emitted by highly conducting Taylor cones," *J. of Fluid Mechanics*, Vol. 260, No., 1994, pp. 155-184.
- ¹⁰ Gamero-Castaño, M., Aguirre-de-Carcer, I., De Juan, L., and Fernández de la Mora, J., "On the current emitted by Taylor cone-jets of electrolytes in vacuo: Implications for liquid metal ion sources," *J. of Appl. Phys.*, Vol. 83, No. 5, 1998, pp. 2428-2434.
- ¹¹ Gamero-Castaño, M., and Fernández de la Mora, J., "Direct measurement of ion evaporation kinetics from electrified liquid surfaces," *J. Chem. Phys.*, Vol. 113, No., 2000, pp. 815-832.
- ¹² Loscertales, I., and Fernández de la Mora, J., "Experiments on the kinetics of field evaporation of small ions from droplets," *J. Chem. Phys.*, Vol. 103, No., 1995, pp. 5041-5060.
- ¹³ Mair, G., "The effects of flow impedance on the current-voltage characteristics of liquid-metal ion sources," *J. of Phys. D: Appl. Phys.*, Vol. 30, No. 13, 1997, pp. 1945.
- ¹⁴ Tajmar, M., "Influence of Taylor cone size on droplet generation in an indium liquid metal ion source," *Appl. Phys. A*, Vol. 81, No. 7, 2005, pp. 1447-1450.
- ¹⁵ Tajmar, M., "Indium capillary liquid-metal-ion-source operation in the flow resistance regime," *J. of Phys. D: Appl. Phys.*, Vol. 37, No. 21, 2004, pp. 3056.
- ¹⁶ Courtney, D.G., and Shea, H., "Influences of porous reservoir Laplace pressure on emissions from passively fed ionic liquid electrospray sources," *Appl. Phys. Lett.*, Vol. 107, No. 10, 2015, pp. 103504.
- ¹⁷ Coffman, C., "Charge emission from electrified ionic liquid menisci: fundamental phenomena and applications to micropropulsion," Ph.D. Dissertation, Massachusetts Institute of Technology, Cambridge, MA, 2016.
- ¹⁸ Coffman, C., Martínez-Sánchez, M., Higuera, F., and Lozano, P.C., "Structure of the menisci of leaky dielectric liquids during electrically-assisted evaporation of ions," *Appl. Phys. Lett.*, Vol. 109, No. 23, 2016, pp. 231602.
- ¹⁹ <http://embedded.eecs.berkeley.edu/pubs/downloads/spice/>, accessed July 28, 2017.
- ²⁰ <http://www.linear.com/solutions/ltspice>, accessed July 28, 2017.
- ²¹ <https://www.sqlite.org/>, accessed July 28, 2017.
- ²² Carrier, W.D., "Goodbye, Hazen; Hello, Kozeny-Carman," *J. of Geotechnical and Geoenvironmental Engineering*, Vol. 129, No. 11, 2003, pp. 1054-1056.
- ²³ Glover, P.W., and Walker, E., "Grain-size to effective pore-size transformation derived from electrokinetic theory," *Geophysics*, Vol. 74, No. 1, 2009, pp. E17-E29.
- ²⁴ Higuera, F.J., "Model of the meniscus of an ionic-liquid ion source," *Physical Review E*, Vol. 77, No. 2, 2008, pp. 026308.
- ²⁵ Forbes, R.G., "Liquid-Metal ion sources and electrosprays operating in cone-jet mode: Some theoretical comparisons and comments," *J. of Aerosol Science*, Vol. 31, No. 1, 2000, pp. 97-120.
- ²⁶ Forbes, R.G., and Ljepojevic, N.N., "Liquid-metal ion source theory: electrohydrodynamics and emitter shape," *Surface Science*, Vol. 266, No. 1-3, 1992, pp. 170-175.
- ²⁷ Tajmar, M., and Genovese, A., "Experimental validation of a mass-efficiency model for an indium liquid-metal ion source," *Appl. Phys. A*, Vol. 76, No. 6, 2003, pp. 1003-1006.
- ²⁸ Perez-Martinez, C., and Lozano, P., "Ion field-evaporation from ionic liquids infusing carbon xerogel microtips," *Appl. Phys. Lett.*, Vol. 107, No. 4, 2015, pp. 043501.
- ²⁹ Gañán-Calvo, A.M., Dávila, J., and Barrero, A., "Current and droplet size in the electrospraying of liquids. Scaling laws," *Journal of Aerosol Science*, Vol. 28, No. 2, 1997, pp. 249-275.
- ³⁰ Gamero-Castaño, M., "Characterization of the electrosprays of 1-ethyl-3-methylimidazolium bis(trifluoromethylsulfonyl) imide in vacuum," *Phys. of Fluids*, Vol. 20, No. 3, 2008, pp. 032103.

- ³¹ Perez-Martinez, C.S., “Engineering ionic liquid ion sources for ion beam applications,” Ph. D. Dissertation, Massachusetts Institute of Technology, Cambridge, MA, 2016.
- ³² Guerra-Garcia, C., Krejci, D., and Lozano, P., “Spatial uniformity of the current emitted by an array of passively fed electro spray porous emitters,” *J. of Phys. D: Applied Physics*, Vol. 49, No. 11, 2016, pp. 115503.
- ³³ Gamero-Castaño, M., and Hruby, V., “Electrospray as a Source of Nanoparticles for Efficient Colloid Thrusters,” *J. of Propulsion and Power*, Vol. 17, No. 5, 2001, pp. 977-987.
- ³⁴ Gamero-Castaño, M., “Characterization of a Six-Emitter Colloid Thruster Using a Torsional Balance,” *J. of Propulsion and Power*, Vol. 20, No. 4, 2004, pp. 736-741.
- ³⁵ Dandavino, S., “Microfabricated Electro spray Thrusters for a Modular Spacecraft Propulsion System,” Ph.D Dissertation, Ecole Polytechnique Federale de Lausanne, Neuchatel, Switzerland, 2014.
- ³⁶ Tajmar, M., and Jang, B., “New materials and processes for field emission ion and electron emitters,” *CEAS Space Journal*, Vol. 4, No. 1-4, 2013, pp. 47-54.
- ³⁷ Reissner, A., Buldrini, N., Seifert, B., Hörbe, T., Plesescu, F., del Amo, J.G., and Massotti, L., “Testing and Modelling of the mN-FEEP Start-Up Performance,” *Proc. 34th International Electric Propulsion Conference and 6th Nano-satellite Symposium*, IEPC-2015-123, Hyogo-Kobe, Japan, July, 2015.
- ³⁸ Vasiljevich, I., Buldrini, N., Plesescu, F., and Schamiloglu, E., “Performance of Porous Tungsten Needle LIMS for Use as Indium FEEP Emitters,” *Proc. 32nd International Electric Propulsion Conference*, IEPC-2011-268, Wiesbaden, Germany, September, 2011.
- ³⁹ Courtney, D.G., Dandavino, S., and Shea, H., “Comparing Direct and Indirect Thrust Measurements from Passively Fed Ionic Electro spray Thrusters,” *Journal of Propulsion and Power*, Vol. 32, No. 2, 2015, pp. 392-407.